View metadata, citation and similar papers at core.ac.uk

brought to you by CORE

provided by Elsevier - Publisher Connector

Available online at www.sciencedirect.com

ScienceDirect

Polar Science 4 (2010) 1–17

NiPR National Institute of Polar Research

http://ees.elsevier.com/polar/

Combined use of InSAR and GLAS data to produce an accurate DEM of the Antarctic ice sheet: Example from the Breivika–Asuka station area

Yamanokuchi Tsutomu [a,b,*], Doi Koichiro [c], Shibuya Kazuo [c]

[a] *Department of Polar Science, Sokendai, Midori-cho 10-3, Tachikawa-city, Tokyo 190-8518, Japan*
[b] *Remote Sensing Technology Center of Japan, 12F, Roppongi First BLDG., 1-9-9, Roppongi, Minato-ku, Tokyo 106-0032, Japan*
[c] *National Institute of Polar Research, Sokendai, Midori-cho 10-3, Tachikawa-city, Tokyo 190-8518, Japan*

Received 26 February 2008; revised 12 November 2009; accepted 25 December 2009
Available online 1 February 2010

Abstract

Surface elevation data for the Breivika–Asuka Station area, East Dronning Maud Land, Antarctica, obtained during ground surveys undertaken in 1987 were compared with elevation data measured by the Geoscience Laser Altimeter System (GLAS) onboard the Ice, Cloud, and land Elevation Satellite (ICESat) in 2003. The two sets of measurements were consistent within ±12.4 m for an elevation range from 300 to 1000 m. We produced an interferometric synthetic aperture radar (InSAR) digital elevation model (DEM) with 50 m grid spacing and InSAR DEM heights were corrected using GLAS heights as ground-truth data. The height differences are assumed to have a quadratic function of rectangular polar stereographic coordinates with six coefficients, and the most probable estimate of the correction parameter set was calculated using a least squares method. Before correction, the root-mean-square (rms) height error was ±284 m; after correction, the associated error was reduced to ±22.3 m, where the absolute error in the horizontal coordinates (grids) was ±230 m. The resultant InSAR DEM height error is twice as large as the GLAS DEM height error; however, the accuracy of the resultant InSAR DEM is reasonable when we consider the limitations of single baseline InSAR and the steep slopes (range in elevation: 1000 m) within the ice sheet region. An InSAR DEM with high spatial resolution and 2 m relative accuracy in terms of yearly change is useful for monitoring ice volume (mass) change by a superconducting gravimeter.
© 2010 Elsevier B.V. and NIPR. All rights reserved.

Keywords: InSAR; GLAS/ICESat; Digital elevation model (DEM); Ground-truth height; Traverse survey

1. Introduction

Synthetic aperture radar interferometry (InSAR) is widely applied in studies of ice dynamics in Antarctica; e.g., to detect ice flow and the grounding line (GL) of glaciers (e.g., Goldstein et al., 1993; Rignot, 1996). Since the early 1990s, many case studies have sought to determine the GL of glaciers,

* Corresponding author at: Remote Sensing Technology Center of Japan, 12F, Roppongi First BLDG., 1-9-9, Roppongi, Minato-ku, Tokyo 106-0032, Japan. Tel.: +81 3 5561 8776; fax: +81 3 5574 8515.
E-mail address: tsutomuy@restec.or.jp (Y. Tsutomu).

1873-9652/$ - see front matter © 2010 Elsevier B.V. and NIPR. All rights reserved.
doi:10.1016/j.polar.2009.12.002

although a review of detailed regional studies is not provided here. We only note that Yamanokuchi et al. (2005) determined the GL that can replace the Antarctic Digital Database (ADD Consortium, 2000) coastline for regions from 5°W to 40°E. The ADD coastline misidentified a peninsula at around 15°E; the InSAR-derived GL revealed that this feature is actually a group of snow-covered islands or ice rises. The InSAR GL also rectified positional discrepancies regarding the ADD coastline; e.g., a 5000 m misfit around Riiser-Larsenhalvøya and a misfit of about 1200 m around Padda and Skallen (see Fig. 1).

From the early stage of its development, InSAR has been directed toward obtaining topographic maps of inaccessible areas (e.g., Zebker et al., 1994). The InSAR technique has also been applied in producing digital elevation models (DEMs; hereafter, such DEMs are referred to as InSAR DEMs). Based on a comparison with airborne laser altimeter data, Joughin et al. (1996) claimed a relative accuracy of 2.5 m for a European Remote Sensing Satellite-1 (ERS-1) DEM for Greenland.

In terms of Antarctica, the Radarsat (Canadian SAR satellite) Antarctic Mapping Project (RAMP) DEM produced by Liu et al. (2001) covers the entire continent with a spatial resolution of 200 × 200 m, although the height accuracy of the model is variable, ranging from ±7.5 m to ±100 m depending on location. This wide range in accuracy arises because of the sparse distribution of ground-control points (GCPs) in areas of bare rock, as GCPs are not always available in inland areas of the Antarctic ice sheet.

Schutz et al. (2005) provided an overview of the Geoscience Laser Altimeter System (GLAS) aboard ICESat (Ice, Cloud, and land Elevation Satellite), which was launched in January 2003. GLAS has been shown to measure the ice sheet topography with a higher accuracy (±14 cm) than that of the ERS-1 radar altimeter (±1 m) (Shuman et al., 2006; Zwally et al., 2003). The recently improved precision of height measurements means that GLAS data are used to resolve, for example, height variability at the GL (Fricker and Padman, 2006), changes in the elevation of ice streams (Csatho et al., 2005), and ice loss (Rignot et al., 2005).

Some of the best examples of the applicability of GLAS data in regional studies include the validation of an InSAR DEM undertaken as part of the Shuttle Radar Topographic Mission (although this did not cover Antarctica; Carabajal and Harding, 2005), and the compilation of an ERS-tandem DEM over the low-relief Arctic coastal plain (Atwood et al., 2007), and the ice shelf of West Antarctica (e.g., Baek et al., 2005). By combining the precise but narrow (line)

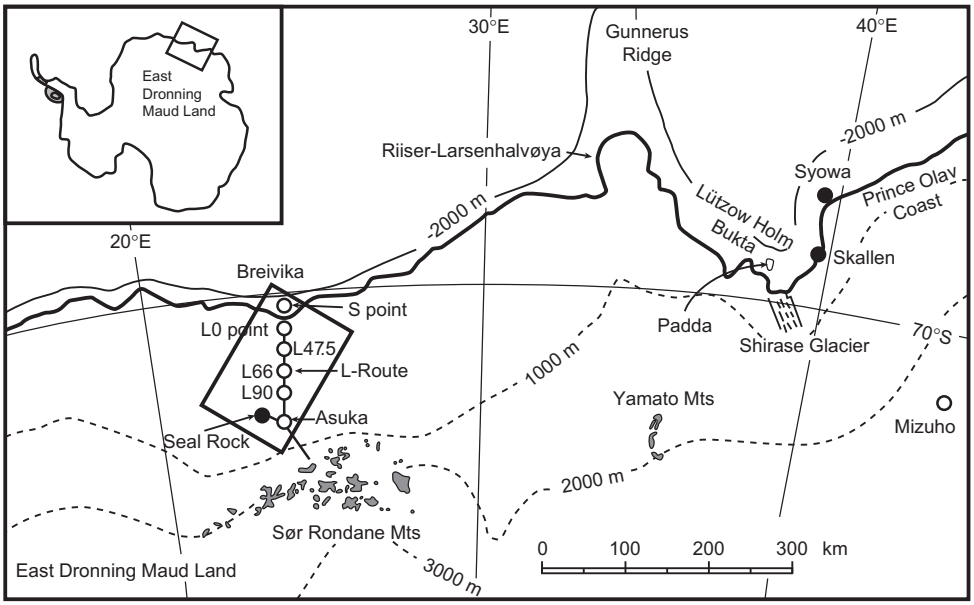

Fig. 1. Simplified topographic map of East Dronning Maud Land, showing the study area (rectangle) in which InSAR DEM were validated using GLAS/ICESat data. A ground-height survey was performed in 1987 along the L-Route between 'L0 point' and Asuka Station (L121), with measurements taken at 1 km intervals using GPS relative positioning, satellite Doppler positioning, and barometric altimeter difference. Solid circles are located on the bare rock area, while open circles are located on the ice sheet.

profile of GLAS data with an InSAR DEM (which has coarse accuracy but wide coverage), it may be possible to produce a more relevant DEM of the Antarctic ice sheet.

We set such a test area, over which to produce a DEM with moderate accuracy and wide coverage, from Asuka Station to Breivika in East Dronning Maud Land, Antarctica (see Fig. 1), for which ground-height survey data are available (Shibuya and Fukuda, 1999). After assessing the height error in the GLAS data based on the ground measurements, we used the DEM grids as reference points (instead of surveyed ground-height data) to control the InSAR DEM heights. The differences between our results and those presented by Baek et al. (2005) are discussed in later sections.

2. Surface-height survey conducted in 1987

In the test area described above (rectangle in Fig. 1), the 28th Japanese Antarctic Research Expedition (JARE-28) conducted a ground-height survey in April 1987 from Asuka Station to 'L0 point' along the L-Route (see Fig. 1) at 1 km intervals. Since this survey, there have been no ground-height surveys of sufficient accuracy until the present study. We utilized all the available surface-height data obtained by various methods during the survey, including satellite Doppler positioning, GPS relative positioning, and height differences measured using a barometric altimeter. Detailed positioning results can be found in Shibuya et al. (1990, 1991, 1999); here, we only describe the methodology and assessment of measurement accuracy.

Fig. 2 shows the various methods used to determine the height (above mean sea level) at 'L0 point'. Broadcast ephemeris satellite Doppler positioning using 94 passes, as acquired by a JMR-4A receiver (JMR Instruments Inc., 1977), at 'L0 point' yielded a convergence error of ±0.24 m for the ellipsoidal height H_0 (but with a probable absolute error of 4 m). A SONY GTT-3000 L1 (C/A code) frequency four-channel tracking GPS receiving system (Fujita et al., 1987) was installed at each end of the baseline that extended from the GPS antenna near 'L0 point' ('pseudo-L0 point') to that on the icebreaker *Shirase* ('S point'). Simultaneous GPS receiving was made from 1730 to 1840 Universal time (UT) on 23 December 1986; data analysis revealed a height difference h with an accuracy of ±0.3 m. In December 1986, when the GPS observations were made, only five satellites were in operation, and the four satellites in view were available for about 8 h per day. Therefore,

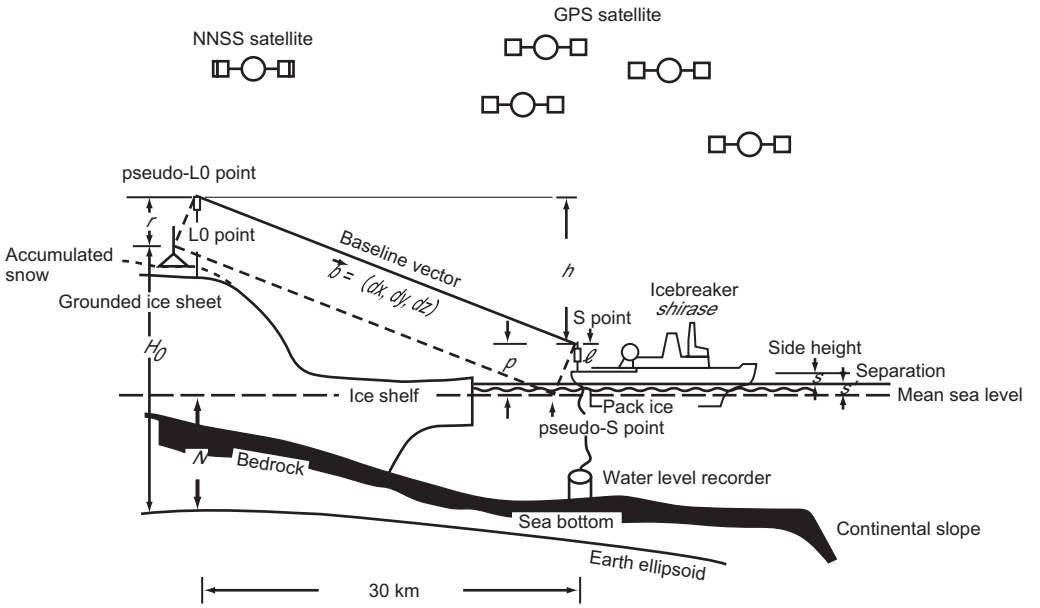

Fig. 2. Determination of geoid height at 'S point' in Breivika (see Fig. 1) and elevation above sea level at 'L0 point' (30 km from 'S point'). Modified from Fig. 2 of Shibuya et al. (1991) and see the text for details. H_0: Ellipsoidal height of 'L0 point'; N: Geoid height at 'L0 point'; h: Height difference between 'pseudo-L0 point' and 'S point'; p: Separation of 'S point' from the mean sea level; ℓ: Height of 'S point' from the deck; s: Side height of the deck from the then sea level; s': Separation of the then sea level from the mean sea level; r: Height offset of the 'pseudo-L0 point' from that of 'L0 point'; (dx, dy, dz): Baseline vector components from 'L0 point' to 'S point'.

the field operations were conducted under severe logistical restrictions. An Aanderaa WLR-7 (Bergen model) pressure-transducer water-level recorder was installed on the sea floor at a depth of 200 m, at the anchoring site of the icebreaker *Shirase* in Breivika. Sea level change was measured for 4 days at a sampling interval of 10 min, and the separation of sea surface height from the local mean sea level during the period of GPS observations (s' in Fig. 2) was obtained with an accuracy of ±0.3 m.

Based on measurements of 'S point' offset above the deck (ℓ in Fig. 2) and side height s above the then sea level, the height offset of 'S point' from the local mean sea level ($p = \ell + s + s'$) (see Fig. 2) was measured with ±0.3 m accuracy. Because both the GPS and satellite Doppler antennas were located close to 'L0 point', their difference in height (r in Fig. 2) involved an error of within several centimeters.

Shibuya et al. (1991) obtained the geoid height N at 'S point' (here assumed to be equal to the geoid height at 'L0 point', given the short distance of ~30 km between the points) as

$$N = H_0 - h - p + r = 186.0 - 162.5 - 7.4 + 0.72 = 16.8\,\mathrm{m}; \quad (1)$$

however, by assuming a zero value for sea surface topography ζ. Shibuya et al. (1999) updated the estimate as follows:

$$N = H_0 - h - p + r - \zeta = 190.0 - 162.5 - 7.4 + 0.72 + 1.43 = 22.3\,\mathrm{m}, \quad (1)'$$

on the WGS84 Ellipsoid, where H_0 was replaced with the precise ephemeris positioning result of 79 passes, and sea surface topography $\zeta = -1.43$ m was adopted for 'S point' (e.g., Lemoine et al., 1997). The accuracy of the obtained geoid height is estimated to be within 2 m.

During the surface-height survey performed along the L-Route, satellite Doppler translocation and/or GPS relative positioning were conducted at 20–30 km intervals with a resultant height accuracy of 2 m at L47.5, L66, L90, Asuka Station, and Seal Rock (see Fig. 1). Although surface heights at other points were interpolated based on barometric altimeter readings, the same 2 m accuracy is assumed for these height measurements taken at 1 km intervals because of the short time interval (typically within 30 min) between measurements at neighboring points.

In summary, Table 1 (column 4) shows the basic surface-height measurements (2 m accuracy) above mean sea level, where the geodetic coordinates (columns 2–3) are given in the WGS84 reference system. To convert these surface elevations to ellipsoidal heights (column 5), ground (not modeled) geoid height data at 'L0 point' (22.3 m) and Seal Rock (21.4 m) were added by adjusting for EGM96 model undulations (Lemoine et al., 1997).

3. Estimate of surface heights in 2003

A period of 16 years elapsed between the ground traverse survey in April 1987 and the GLAS measurements, which started in February 2003; consequently, it is necessary to correct for changes in surface height over this period due to snow accumulation/ablation.

Fig. 3 shows monthly measurements of snow accumulation at Asuka Station since the ground-height survey during April 17–22 1987; raw data measured at the 36-pole snow-stake farm were published in JARE Data Reports from 1987 through 1991 (Fujii et al., 1995; Nishio and Ohmae, 1989; Watanabe et al., 1990). As shown in Fig. 3, the period from late December to late April is the season of snow accumulation, while late June to late December is marked by minor ablation or no change. We recognize years with an annual accumulation rate of 21–22 cm/yr (1988–1989 and 1989–1990) and those with a rate of 66–76 cm/yr (1987–1988 and 1990–1991), with an average rate of 46.3 cm/yr for the 4 years.

Fig. 4 shows two photographs of the same 1 kW wind-generator at Asuka Station: the upper photograph was taken on 14 January 1991, immediately after installation of the generator by the JARE-32 winter-over Asuka party, and the lower photograph was taken on 1 December 2004 by the short-visit Sør Rondane (see Fig. 1) summer party. Using the pole upon which the wind-generator is mounted as a reference for measuring the level of the snow surface, the burial depth d during the 14-year period between the photographs was 2.1 m. The total thickness of accumulated snow during this interval can be considered as H = 46.3 cm/yr × 14 years = 6.5 m.

Superficial accumulated snow is subjected to compaction, and the compaction factor can be reasonably estimated as

$$c = d/H = 2.1\,\mathrm{m}/6.5\,\mathrm{m} = 0.32. \quad (2)$$

Table 1
Ground-survey heights along the L-Route, as measured in 1987, and corrected heights of snow accumulation. Column 5, ellipsoidal height in 1987; column 6, ellipsoidal height in 2003 after the correction of snow accumulation and surface subsidence; column 7, interpolated GLAS height using GLAS/ICESat 500 m DEM grids; column 8, height difference (column 7 minus column 6).

Column 1	Column 2	Column 3	Column 4	Column 5	Column 6	Column 7	Column 8
Station name	Latitude (°)	Longitude (°)	Surface elevation in 1987 (m)	Ellipsoidal height in 1987 (m)	Ellipsoidal height in 2003 (m)	Interpolated GLAS height in 2003 (m)	Difference (7)-(6)
L0	−70.454	23.890	168.0	190.3			
L1	−70.463	23.890	177.0	199.3			
L2	−70.472	23.890	188.0	210.3	212.2	105.7	−106.5
L3	−70.482	23.891	196.0	218.3	220.5	125.5	−95.0
L4	−70.490	23.891	205.0	227.3	228.7	137.4	−91.3
L5	−70.500	23.891	211.0	233.3	235.0	155.5	−79.5
L6	−70.508	23.892	218.0	240.3	241.3	174.4	−66.9
L7	−70.517	23.892	231.0	253.3	254.4	190.2	−64.2
L8	−70.527	23.892	244.0	266.3	267.5	221.5	−46.0
L9	−70.535	23.893	247.0	269.3	271.4	219.8	−51.6
L10	−70.545	23.893	250.0	272.3	275.3	230.5	−44.8
L11	−70.553	23.894	253.0	275.3	278.2	238.8	−39.4
L12	−70.562	23.894	256.0	278.2	281.1	257.6	−23.5
L13	−70.572	23.894	240.0	262.2	264.6	260.5	−4.1
L14	−70.580	23.896	224.0	246.2	248.1	260.9	12.8
L15	−70.590	23.898	218.0	240.2	242.0	260.0	18.0
L16	−70.598	23.898	211.0	233.2	235.9	264.3	28.4
L17	−70.608	23.898	209.0	231.2	234.8	262.9	28.1
L18	−70.617	23.899	208.0	230.2	233.7	261.5	27.8
L19	−70.627	23.899	211.0	233.2	236.7	260.3	23.6
L20	−70.635	23.899	214.0	236.2	239.6	259.3	19.7
L21	−70.643	23.901	215.0	237.2	240.0	260.8	20.8
L22	−70.653	23.901	216.0	238.2	240.4	260.2	19.8
L23	−70.662	23.901	217.0	239.2	241.7	260.0	18.3
L24	−70.672	23.901	218.0	240.2	242.9	262.3	19.4
L25	−70.680	23.903	216.0	238.1	240.9	263.6	22.7
L26	−70.688	23.903	214.0	236.1	238.8	266.6	27.8
L27	−70.698	23.903	219.0	241.1	242.3	270.6	28.3
L28	−70.707	23.904	221.0	243.1	245.7	275.6	29.9
L29	−70.717	23.904	227.0	249.1	252.6	281.5	28.9
L30	−70.725	23.904	234.0	256.1	259.5	285.2	25.7
L31	−70.733	23.906	234.0	256.1	259.6	290.8	31.2
L32	−70.743	23.906	234.0	256.1	259.7	297.9	38.2
L33	−70.752	23.906	244.0	266.1	269.2	305.5	36.3
L34	−70.762	23.906	254.0	276.1	278.7	313.5	34.8
L35	−70.770	23.207	260.0	282.1	284.4	319.4	35.0
L36	−70.778	23.908	266.0	288.1	290.1	324.2	34.1
L37	−70.788	23.908	280.0	302.0	304.4	331.9	27.5
L38	−70.797	23.909	294.0	316.0	318.7	339.6	20.9
L39	−70.807	23.909	300.0	322.0	324.5	347.2	22.7
L40	−70.815	23.910	306.0	328.0	330.2	354.2	24.0
L41	−72.823	23.912	316.0	338.0	340.4	358.7	18.3
L42	−70.833	23.912	326.0	348.0	350.5	369.4	18.9
L43	−70.842	23.913	340.0	362.0	364.0	378.1	14.1
L44	−70.850	23.914	354.0	376.0	377.5	381.9	4.4
L45	−70.860	23.914	360.0	382.0	383.3	390.1	6.8
L46	−70.868	23.915	366.0	388.0	389.1	397.4	8.3
L47	−70.877	23.916	384.0	406.0	404.8	404.3	−0.5
L47.5	−70.882	23.916	387.0	409.0			
L48	−20.887	23.916	396.0	418.0	420.4	409.8	−10.6
L49	−70.895	23.916	403.0	424.9	427.5	415.9	−11.6
L50	−70.905	23.916	410.0	431.9	434.6	422.3	−12.3

(*continued on next page*)

Table 1 (*continued*)

Column 1	Column 2	Column 3	Column 4	Column 5	Column 6	Column 7	Column 8
Station name	Latitude (°)	Longitude (°)	Surface elevation in 1987 (m)	Ellipsoidal height in 1987 (m)	Ellipsoidal height in 2003 (m)	Interpolated GLAS height in 2003 (m)	Difference (7)-(6)
L51	−70.913	23.916	417.0	438.9	442.0	425.9	−16.1
L52	−70.922	23.916	424.0	445.9	449.4	432.9	−16.5
L53	−70.932	23.915	430.0	451.9	455.1	440.1	−15.0
L54	−70.940	23.915	436.0	457.9	460.8	446.9	−13.9
L55	−70.950	23.915	443.0	464.9	468.2	454.5	−13.7
L56	−70.958	23.915	450.0	471.9	475.5	458.5	−17.0
L57	−70.967	23.916	457.0	478.9	482.1	466.3	−15.8
L58	−70.977	23.918	464.0	485.9	488.7	474.1	−14.6
L59	−70.985	23.918	471.0	492.9	496.1	482.3	−13.8
L60	−70.993	23.920	478.0	499.9	503.4	490.6	−12.8
L61	−71.003	23.921	484.0	505.8	509.2	521.4	12.2
L62	−71.012	23.923	490.0	511.8	515.0	524.1	9.1
L63	−71.020	23.924	495.0	516.8	519.9	527.9	8.0
L64	−71.028	23.924	500.0	521.8	524.7	527.1	2.4
L65	−71.038	23.925	506.0	527.8	530.5	523.2	−7.3
L66	−71.048	23.927	511.0	532.8	536.2	522.6	−13.6
L67	−71.056	23.927	515.0	536.8	540.4	541.6	1.2
L68	−71.065	23.929	519.0	540.8	544.5	548.6	4.1
L69	−71.073	23.931	528.0	549.8	553.2	552.8	−0.4
L70	−71.083	23.931	537.0	558.8	561.8	560.1	−1.7
L71	−71.092	23.931	544.0	565.8	568.9	567.1	−1.8
L72	−71.100	23.931	551.0	572.8	575.9	572.6	−3.3
L73	−71.110	23.929	560.0	581.7	583.6	577.9	−5.7
L74	−71.118	23.929	567.0	588.7	591.2	581.6	−9.6
L75	−71.128	23.927	571.0	592.7	596.5	587.7	−8.8
L76	−71.137	23.927	578.0	599.7	601.7	595.4	−6.3
L77	−71.145	23.927	587.0	608.7	611.0	605.0	−6.0
L78	−71.155	23.929	596.0	617.7	620.3	610.9	−9.4
L79	−71.163	23.929	600.0	621.7	624.3	614.2	−10.1
L80	−71.173	23.931	604.0	625.7	628.3	626.2	−2.1
L81	−71.182	23.933	613.0	634.7	636.5	640.7	4.2
L82	−71.190	23.933	622.0	643.7	644.7	646.6	1.9
L83	−71.200	23.935	629.0	650.7	653.3	652.3	−1.0
L84	−71.208	23.935	636.0	657.7	661.9	656.8	−5.1
L85	−71.218	23.937	646.0	667.6	670.5	675.4	4.9
L86	−71.227	23.937	656.0	677.6	679.1	688.3	9.2
L87	−71.235	23.939	665.0	686.6	687.1	693.6	6.5
L88	−71.245	23.939	672.0	693.6	695.1	697.5	2.4
L89	−71.253	23.941	676.0	697.6	699.3	699.0	−0.3
L90	−71.262	23.941	680.0	701.6	703.5	700.8	−2.7
L91	−71.272	23.941	687.0	708.6	709.0	707.5	−1.5
L92	−71.280	23.942	694.0	715.6	714.4	718.6	4.2
L93	−71.288	23.942	697.0	718.6	718.9	721.8	2.9
L94	−71.298	23.942	700.0	721.6	723.3	726.6	3.3
L95	−71.307	23.943	703.0	724.6	726.1	732.2	6.1
L96	−71.315	23.943	706.0	727.6	728.8	736.3	7.5
L97	−71.325	23.943	709.0	730.5	731.7	738.6	6.9
L98	−71.333	23.943	712.0	733.5	734.5	743.4	8.9
L99	−71.343	23.945	719.0	740.5	741.1	750.1	9.0
L100	−71.352	23.945	726.0	747.5	747.6	757.0	9.4
L101	−71.360	23.957	726.0	747.5	748.0	763.7	15.7
L102	−71.367	23.968	726.0	747.5	748.4	767.4	19.0
L103	−71.375	23.978	733.0	754.5	756.0	775.9	19.9
L104	−71.400	23.990	740.0	761.5	763.6	798.3	34.7
L105	−71.390	24.002	753.0	774.5	776.2	793.5	17.3
L106	−71.398	24.013	766.0	787.5	788.7	800.6	11.9

Table 1 (*continued*)

Column 1	Column 2	Column 3	Column 4	Column 5	Column 6	Column 7	Column 8
Station name	Latitude (°)	Longitude (°)	Surface elevation in 1987 (m)	Ellipsoidal height in 1987 (m)	Ellipsoidal height in 2003 (m)	Interpolated GLAS height in 2003 (m)	Difference (7)-(6)
L107	−71.405	24.025	773.0	794.5	796.3	806.2	9.9
L108	−71.413	24.035	780.0	801.5	803.9	812.4	8.5
L109	−71.422	24.047	777.0	798.4	805.1	814.7	9.6
L110	−71.428	24.058	784.0	805.4	806.3	815.1	8.8
L111	−71.438	24.065	791.0	812.4	812.8	820.9	8.1
L112	−71.447	24.070	798.0	819.4	819.3	841.0	21.7
L113	−71.455	24.077	811.0	832.4	832.4	848.1	15.7
L114	−71.463	24.083	824.0	845.4	845.4	871.0	25.6
L115	−71.472	24.090	842.0	863.4	864.0	884.5	20.5
L116	−71.480	24.095	860.0	881.4	882.5	897.1	14.6
L117	−71.490	24.102	873.0	894.4	895.6	909.2	13.6
L118	−71.498	24.108	886.0	907.4	908.6	925.1	16.5
L119	−71.507	24.113	909.0	930.4	931.2	949.5	17.4
L120	−71.516	24.120	932.0	953.4	953.8	968.3	14.5
L121	−71.525	24.126	956.0	977.4	979.5	981.6	2.1
SEAL	−71.525	24.065	974.0	995.4	995.4	965.3	−30.1

Another factor that affects change in surface height is subsidence related to ice sheet flow. The amount of surface subsidence resulting from laminar flow is controlled by the regional-scale slope of the ice sheet. In the study region, the slope α is represented by the height difference between L121 and L13 in Table 1; that is,

$$\tan\alpha = (956.0 - 240.0)\mathrm{m}/(121 - 13)\mathrm{km} = 6.6 \times 10^{-3} \quad (3)$$

Using a typical value of surface flow velocity of $v = 10$ m/yr, the surface subsidence D during $t = 16$ years (from the ground-height survey in 1987 until the beginning of GLAS measurements in 2003) is

$$D = vt\tan\alpha = 10\,\mathrm{m/yr} \times 16\,\mathrm{yr} \times 6.6 \times 10^{-3} = 1\,\mathrm{m}. \quad (4)$$

Accordingly, the net increase in surface elevation I at Asuka Station arising from snow-fall compaction and surface subsidence is estimated to be

$$I = cH - D = 2.1\,\mathrm{m} - 1.0\,\mathrm{m} = 1.1\,\mathrm{m}. \quad (5)$$

Along the L-Route, snow accumulation was also measured by the Asuka wintering parties; Table 2 (columns 2–5) lists the raw data compiled from Nishio and Ohmae (1989), Watanabe et al. (1990), and Fujii et al. (1995). Column 6 gives the total accumulation over a period of 1–4 years (the number of years

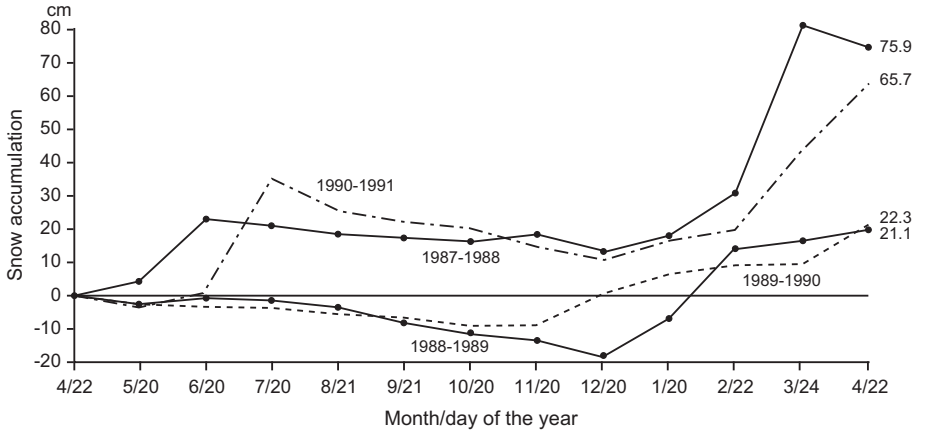

Fig. 3. *In situ* measurements of snow accumulation at Asuka Station, as measured from a 36-pole snow-stake farm. Yearly data are plotted for the 4-year period from 22 April 1987 to 22 April 1991.

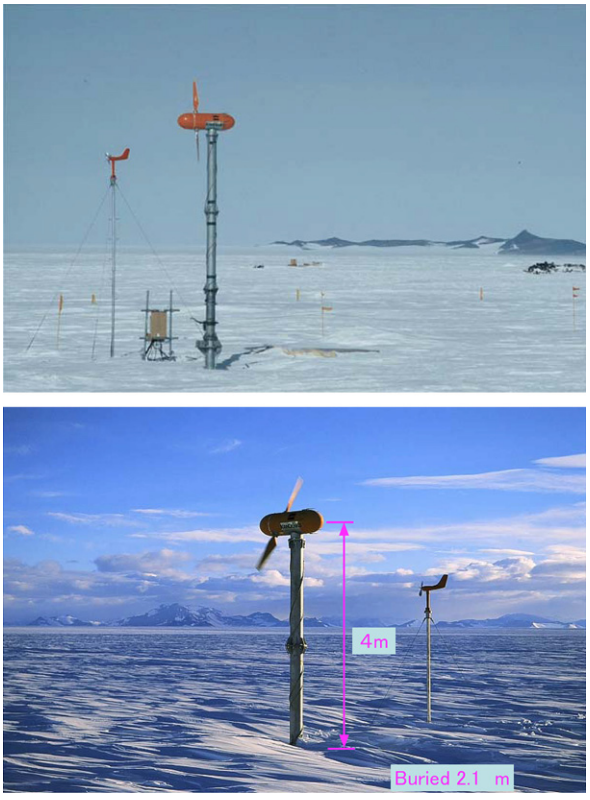

Fig. 4. Comparison of the level of the snow surface against the pole supporting a 1 kW wind-generator, between 14 January 1991 (top panel) and 1 December 2004 (bottom panel), indicating a burial depth of 2.1 m over the 14-year interval between the two photographs. The extrapolated amount of snow accumulation indicated by *in situ* measurements was 6.5 m, indicating a compaction factor of 0.32. This value was adopted for measurements of snow accumulation along the L-Route (Table 2).

is given in parentheses in the table), and column 7 gives the average annual accumulation rate.

By applying Eq. (2) and Eq. (4) to the case of the 36-pole snow-stake farm at Asuka Station, we calculated the net accumulation I at each route point over the period of 16 years (column 8 in Table 2), thickness D after compaction (column 9), and increase in surface elevation (column 10).

In a study of the 0–30°E area (herein referred to as A–A′), Wingham et al. (1998) reported a mean equivalent ice (0.917 g/cm^3) accumulation rate of 10 cm/yr with equivalent snow (0.35 g/cm^3) fall variability of 1.9 cm/yr. Because the test area in Fig. 1 is located coastward of the A–A′ region, the *in situ* measurements (column 7 in Table 2) are 100–200% larger than the above mentioned snow-fall rate given by 10 cm/yr × 0.917/0.35 = 26.2 cm/yr.

By adding column 10 in Table 2 to column 5 in Table 1, we obtain the predicted surface elevation in ellipsoidal height (column 6 in Table 1) in 2003, when the GLAS/ICESat measurements first started. As the amount of snow accumulation was measured at 2 km intervals for the even-numbered poles, surface heights at odd-numbered poles were obtained by averaging the heights at the two neighboring even-numbered poles.

4. Comparison of ground-survey heights with GLAS/ICESat heights

Fig. 5 shows the profiles of GLAS ground footprints (green and red lines numbered 1–10) in the test area, which are confined to within latitudes of 70°50′S to 71°25′S, and within longitudes of 22°40′E to 24°30′E. The profiles cover the data obtained by lasers 2b, 2c, and 3a during 2004 (see Table 3).

Because the closest GLAS profiles (lines 2, 8, and 10 in Fig. 5) to the ground-survey transect (yellow dots) are all oriented oblique, it is not possible to compare ground-survey heights with adjacent GLAS heights directly. We initially considered that east–west variations in surface topography would be one to two orders of magnitude smaller than the north–south-trending slope (using Eq. (3): $\alpha = 6.6 \times 10^{-3}$) and that the simple geometrical average of neighboring GLAS points would give the approximate GLAS height corresponding to the ground-survey height; however, trial calculations revealed a large error that varied depending on the combination of selected neighboring points.

Consequently, we used the GLAS/ICESat 500 m Laser Altimetry Digital Elevation model of Antarctica (Data Set ID: NSIDC-0304), as downloaded from the National Snow and Ice Data Center (NSIDC), USA (DiMarzio et al., 2007). This DEM was produced by averaging all the data by temporal coverage from February 2003 to June 2005 (lasers 1a, 2a, 2b, 2c, 3a, 3b, and 3c in Table 3).

The original GLAS point data have a footprint of 70 m, sampling interval of 170 m for an along-track direction, and span interval of 2500 m for a cross-track direction, nominally at the latitude of 80°S. The track density becomes sparser (and accuracy decreases) toward the equator. Following the description of "derivation technique and algorithms" provided in DiMarzio et al. (2007), a bi-quadratic surface was fitted to all elevations with a circular region surrounding each grid node (called a "cap"). To define the GLAS grid height, the weighted mean of the spot elevations within each cap was calculated by assigning a weighting that was inversely proportional to the square of the distance from the spot to the center

Table 2
Snow accumulation and elevation increase along the L-Route. Column 1, station name; columns 2−5, *in situ* measurements of snow accumulation for the indicated time interval; column 6, total accumulated snow during the year(s) indicated in parentheses; column 7, accumulation rate of snow; column 8, total accumulation of snow I over 16 years assuming the rate in column 7; column 9, thickness of snow D after compaction; column 10, increase in the elevation of the snow surface given the combined effect of an increase in snow thickness and subsidence arising from ice sheet flow.

Column 1	Column 2	Column 3	Column 4	Column 5	Column 6	Column 7	Column 8	Column 9	Column 10
	Feb-Dec1987 (309 days)	Dec1987−Sep 1988 (274 days)	Sep1988−Oct 1989 (393 days)	Oct1989−Oct 1990 (363 days)	Total accumulation* (cm)	Accumulation rate (cm/yr)	Accumulation/ in 16 years (cm)	Thickness D after compaction (m)	Elevation increase (m)
L2	56				56 (1)	56	896	2.9	1.9
L4	46				46 (1)	46	736	2.4	1.4
L6	40				40 (1)	40	640	2.0	1.0
L8	43				43 (1)	43	688	2.2	1.2
L10	79				79 (1)	79	1264	4.0	3.0
L12	76				76 (1)	76	1216	3.9	2.9
L14	56				56 (1)	56	896	2.9	1.9
L16	73				73 (1)	73	1168	3.7	2.7
L18	88				88 (1)	88	1408	4.5	3.5
L20	86				86 (1)	86	1376	4.4	3.4
L22	62				62 (1)	62	992	3.2	2.2
L24	73				73 (1)	73	1168	3.7	2.7
L26	72				72 (1)	72	1152	3.7	2.7
L28	70				70 (1)	70	1120	3.6	2.6
L30	85				85 (1)	85	1360	4.4	3.4
L32	90				90 (1)	90	1440	4.6	3.6
L34	71				71 (1)	71	1136	3.6	2.6
L36	59				59 (1)	59	944	3.0	2.0
L38	73				73 (1)	73	1168	3.7	2.7
L40	62				62 (1)	62	992	3.2	2.2
L42	68				68 (1)	68	1088	3.5	2.5
L44	48				48 (1)	48	768	2.5	1.5
L46	41				41 (1)	41	656	2.1	1.1
L48	11	122			133 (2)	66	1056	3.4	2.4
L50	39	94		83	216 (3)	72	1152	3.7	2.7
L52	49	124		91	264 (3)	88	1408	4.5	3.5
L54	48	100		80	228 (3)	76	1216	3.9	2.9
L56	48	126		96	270 (3)	90	1440	4.6	3.6
L58	50	99		72	221 (3)	74	1184	3.8	2.8
L60	34	125		104	263 (3)	88	1408	4.5	3.5
L62	51	105	74	99	329 (4)	82	1312	4.2	3.2
L64	44	88		100	232 (3)	77	1232	3.9	2.9
L66	39	129		90	258 (3)	86	1376	4.4	3.4
L68	47	91	79	149	366 (4)	92	1472	4.7	3.7
L70	63	84	84	85	316 (4)	79	1264	4.0	3.0
L72	53	88		99	240 (3)	80	1280	4.1	3.1
L74	23	71	101	78	273 (4)	68	1088	3.5	2.5
L76	8	88	58	79	233 (4)	58	928	3.0	2.0
L78	45	70	68	97	280 (4)	70	1120	3.6	2.6
L80	46	90	80	67	283 (4)	71	1136	3.6	2.6
L82	−8	64	54	48	158 (4)	40	640	2.0	1.0
L84	83	106		118	307 (3)	102	1632	5.2	4.2
L86	11	75	27	83	196 (4)	49	784	2.5	1.5
L88	0	79	35	79	193 (4)	48	768	2.5	1.5
L90	31	87	29	81	228 (4)	57	912	2.9	1.9
L92	−7	48	6	−58	−11 (4)	−3	−48	−0.2	−1.2
L94	2	98	46	61	207 (4)	52	832	2.7	1.7
L96	45	69	16	36	166 (4)	42	672	2.2	1.2
L98	22	68	19	51	160 (4)	40	640	2.0	1.0

(*continued on next page*)

Table 2 (*continued*)

Column 1	Column 2	Column 3	Column 4	Column 5	Column 6	Column 7	Column 8	Column 9	Column 10
	Feb-Dec1987 (309 days)	Dec1987–Sep 1988 (274 days)	Sep1988–Oct 1989 (393 days)	Oct1989–Oct 1990 (363 days)	Total accumulation* (cm)	Accumulation rate (cm/yr)	Accumulation/ in 16 years (cm)	Thickness *D* after compaction (m)	Elevation increase (m)
L100	−23	82	10	19	88 (4)	22	352	1.1	0.1
L102	46	46	23	33	148 (4)	37	592	1.9	0.9
L104	67	67	37	72	243 (4)	61	976	3.1	2.1
L106	32	32	62	42	168 (4)	42	672	2.2	1.2
L108	78	78	68	44	268 (4)	67	1072	3.4	2.4
L110	58	58	9	21	146 (4)	37	592	1.9	0.9
L112	4	4	17	43	68 (4)	17	272	0.9	−0.1
L114	26	26	−1	28	79 (4)	20	320	1.0	0.0
L116	33	33	52	45	163 (4)	41	656	2.1	1.1
L118	74	74	5	13	166 (4)	42	672	2.2	1.2
L120	45	45	5	13	108 (4)	27	432	1.4	0.4

*Numbers in parentheses indicate the years of total accumulation'.

of the grid node. It is noted that for Antarctica, the cap size ranged from 2 to 20 km (DiMarzio et al., 2007).

Based on the 500 m DEM grids, the GLAS height at each ground-survey point was calculated by again applying a bi-quadratic interpolation of spot elevations within 2 km of each point. The resultant GLAS ellipsoidal heights are listed in column 7 of Table 1, and are plotted as blue dots in Fig. 6 (scale on left-hand axis), together with the ground-survey ellipsoidal heights (column 6 in Table 1) which are plotted as red dots. The difference in heights (i.e., column 7 minus column 6) is listed in column 8 and plotted as green

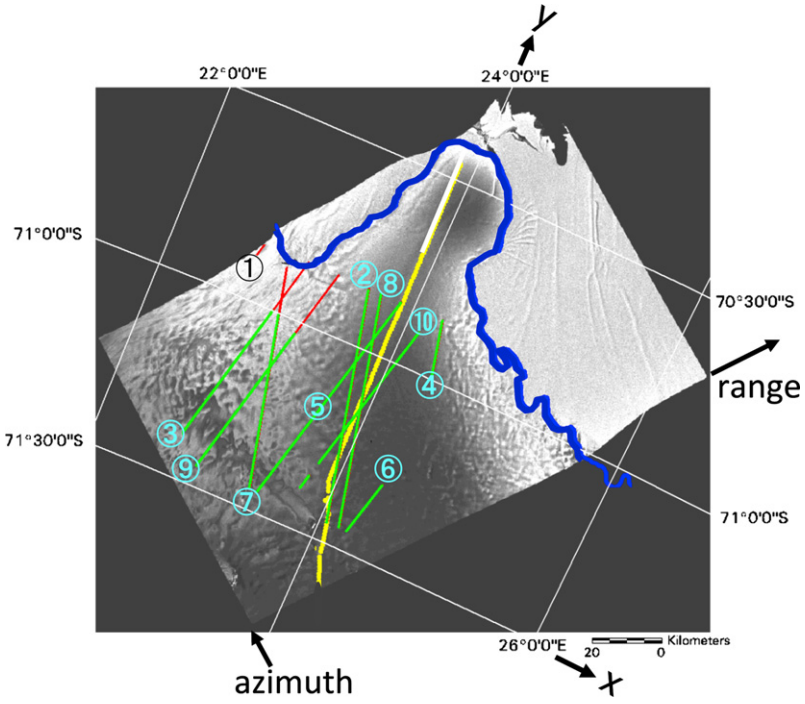

Fig. 5. SAR intensity image showing the locations of GLAS profiles (green lines) in the study area. Red segments indicate poor accuracy due to high flow velocity. Range–azimuth coordinates are rotated anticlockwise by about 35° compared with the x–y polar stereographic coordinates. Yellow dots indicate the route of the ground traverse undertaken by JARE-28, and the blue line indicates the coastline. The DEM grids of the GLAS/ICESat 500 m Laser Altimetry Digital Elevation model of Antarctica (Data Set ID: NSIDC-0304) by DiMarzio et al. (2007) were not shown but they are distributed in the scene.

Table 3
Details of the GLAS/ICESat dataset used for validating the InSAR DEM.

Laser code	Period	Repetition interval
1a	20 Feb.–29 Mar. 2003	8 day
2a	25 Sep.–19 Nov. 2003	33 day subcycle
2b	17 Feb.–21 Mar. 2004	33 day subcycle
2c	17 May–19 June 2004	33 day subcycle
3a	4 Oct.–8 Nov. 2004	33 day subcycle
3b	17 Feb.–22 Mar. 2005	33 day subcycle
3c	20 May–23 June 2005	33 day subcycle

dots in Fig. 6 (scale on the right-hand axis). The difference was largely negative from L2 to L13 (190–240 m elevation), but was moderately positive (13–38 m) from L14 to L37 (240–280 m elevation). From L38 to L121 (Asuka Station), the difference varied within a stable range of about ±20 m.

As summarized in Table 4, the standard error of the above differences is ±44.2 m for L2–L37, in the area of lower elevation (<300 m), and ±12.4 m for L38–L121, in the area of higher elevation (300–1000 m). The error for the entire L-Route was ±26.3 m. This result encourages us to use the GLAS DEM grids (in place of ground-survey heights) as reference points to control InSAR DEM.

5. Procedure for InSAR DEM production and calibration by GLAS data

Fig. 7 shows the procedure followed for the production and calibration/correction of the InSAR DEM. We used the European Remote Sensing Satellites-1/-2 (ERS-1/-2) tandem pair for 21–22 May 1996, as received at Syowa Station (Fig. 1). The pair covered the test area of Breivika–Asuka Station (see the rectangle in Fig. 1), with the perpendicular component of the baseline length $Bp = 37$ m. To obtain an accurate DEM, Bp should be much longer than 37 m, although when Bp becomes too long, deformation fringes resulting from high flow rates of the surface ice sheet near the coastline are greatly enhanced, along with greater spatial decorrelation. Therefore, the value of Bp must be selected by considering the tradeoff between these two effects. In the present case, we found only one data pair from the ERS-1/ERS-2 archive available over the study area.

We created an interferogram from this pair and performed phase unwrapping (step 1 in Fig. 7) using a Gamma Interferometric SAR processor (Gamma Remote Sensing, 2007); the phase-unwrapped interferogram is shown in Fig. 8. The DEM after phase unwrapping has coordinates in the SAR range–azimuth system, and contains distortion such as foreshortening and layover (e.g., Hanssen, 2001). We then made an ortho-rectified DEM and an ERS-1 intensity image; these data sets have no geodetic coordinates at this stage (step 2).

Similar to the procedure followed in detecting the grounding line from InSAR scenes (Yamanokuchi et al., 2005), we referred to a RAMP image downloaded from NSIDC (Liu et al., 2001). A RAMP image is a SAR mosaic with 125 m spatial resolution and that

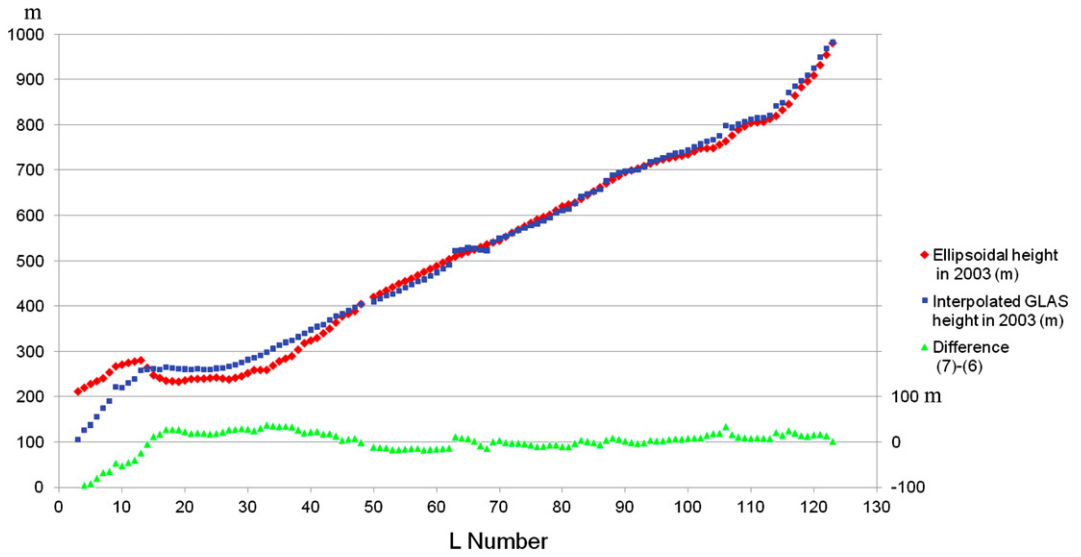

Fig. 6. GLAS ellipsoidal heights (blue squares) compared with ground-survey ellipsoidal heights (red diamonds) along the L-Route (scale: left-hand axis). The difference between the two data sets is shown by green triangles (scale: right-hand axis). (For interpretation of the references to colour in this figure legend, the reader is referred to the web version of this article.)

Table 4
Summary of the height differences between InSAR DEM and GLAS DEM along the ground-survey route. The rms difference for the L2–L37 portion (0–300 m elevation) is four times larger than that for the L38–L121 portion (300–1000 m elevation).

Location	Height (m)	GLAS DEM − Ellipsoidal height (m)	InSAR DEM − GLAS DEM (m)
L2–L37	<300	±44.2	−84.0 (average bias)
L38–L121	300–1000	±12.4	±22.3
L2–L121	0–1000	±26.3	±49.7

is ortho-rectified in the associated WGS84 geodetic coordinates. The RAMP images were projected into the polar stereographic rectangular (x, y) system with the standard parallel at 71°S, which we resampled at 50 m/pixel to ensure equivalence with the ERS image and InSAR fringe sizes. With reference to at least seven GCPs, the WGS84 geodetic coordinates can be allocated to the processed InSAR DEM grids by referring to the RAMP mosaic (step 3). The scene contains nine GCPs.

The GLAS/ICESat data were given on the reference ellipsoid with an equatorial radius a of 6378136.30 m and reciprocal flattening $1/f$ of 298.257, which we transformed into the WGS84 geodetic coordinate height G_i (x_i, y_i), and obtained the corresponding InSAR DEM height S_i (x_i, y_i), where i denotes the integer that specifies the grid position.

The associated height error $\breve{Z}_i$ (x_i, y_i) can then be expressed by (step 4)

$$\breve{Z}_i(x_i, y_i) = S_i(x_i, y_i) - G_i(x_i, y_i). \quad (6)$$

We assume that the height error $\breve{Z}_i$ (x_i, y_i) can be modeled by a bi-quadratic function with six coefficients (a–f):

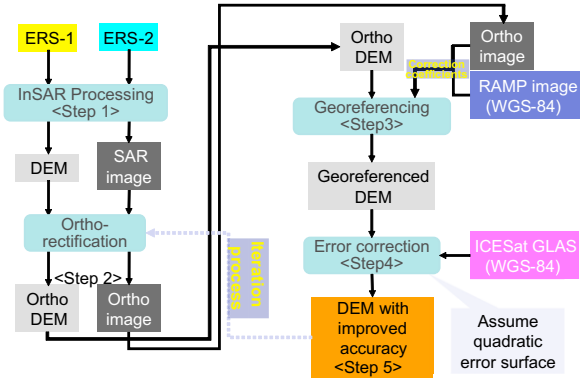

Fig. 7. Procedure followed in producing the InSAR DEM, and correction for the associated height error using GLAS/ICESat data. For details, see the main text.

$$\mathrm{q}(\mathrm{x}, \mathrm{y}) = ax^2 + bx + cxy + dy + ey^2 + f. \quad (7)$$

The most probable estimate for the set of coefficients a_0–f_0 can be obtained by the least squares error method:

$$V^{\mathrm{dif}} = \sum [\breve{Z}_i(x_i, y_i) - q(x_i, y_i)]^2 = \min. \quad (8)$$

Thus, the estimated most probable correction function q_0 (x, y) with the determined coefficients a_0–f_0 can be integrated to obtain highly accurate InSAR DEM $\mathrm{NS_i}$ (step 5 in Fig. 7), which is given by

$$NS_i(x_i, y_i) = S_i(x_i, y_i) - q_0(x_i, y_i), \quad (9)$$

with

$$q_0(x_i, y_i) = a_0 x_i^2 + b_0 x_i + c_0 x_i y_i + d_0 y_i + e_0 y_i^2 + f_0. \quad (10)$$

6. Comparison of InSAR DEM heights with GLAS heights

Fig. 9 shows the InSAR DEM heights obtained by stepwise correction using the GLAS heights. The GLAS heights are interpolated from the 500 m DEM grids (DiMarzio et al., 2007) and plotted on profiles 2–10 (see Fig. 5) using red dots. The InSAR DEM heights on the corresponding GLAS profiles are also interpolated from the InSAR 50 m DEM grids, and are plotted in Fig. 9 by dark blue dots.

Several portions of the obtained InSAR DEM height profiles (profile 1, red segments of profiles 3, 7, and 9 in Fig. 5) show the opposite trends to those in GLAS height. These portions are located close to the coastline (blue line in Fig. 5), which is marked by high flow velocities of the ice sheet. As a result, the InSAR fringes related to ice flow are likely to overlap with the topographic fringes, introducing errors into the InSAR DEM heights. Therefore, we removed these segments from subsequent analyses.

In Fig. 9, the discrepancies between the InSAR DEM heights (dark blue dots) and GLAS heights (red dots) range from 200 to 400 m; the average rms value is 284 m (note that in the figure, the blue curve is always above the red curve). The bias-removed InSAR DEM height profile (light blue dots) deviates from the GLAS height profile with an rms error of ±85.4 m. Generally, the InSAR DEM heights fall below the GLAS DEM heights toward lower elevations, with the crossover occurring at close to the mid-point along the profile at around 500–600 m height. This trend may be related to

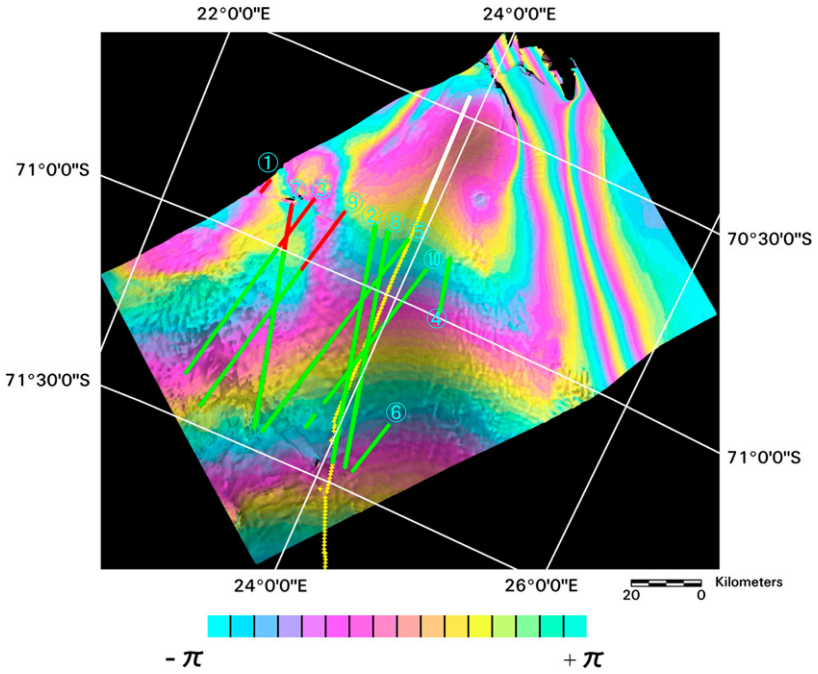

Fig. 8. Phase-unwrapped interferogram of the study area (corresponding to the area shown in Fig. 5).

the distortion of topographic fringes in the lower-elevation area, which is affected by uncorrected ice flow and orbit fringes, and related in part to the unstable nature of satellite dynamics in measuring laser tracking for the steep north–south undulations (i.e., parallel to GLAS profiles) of the ice sheet.

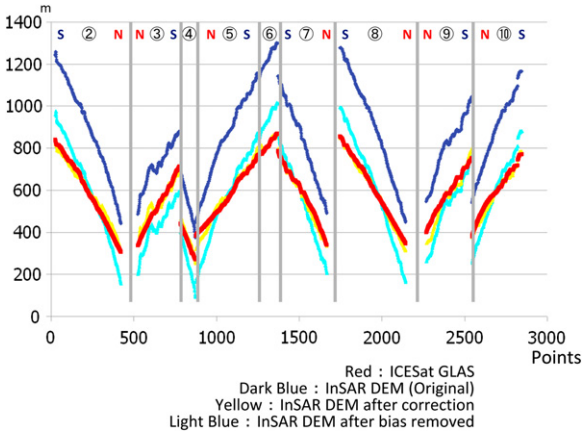

Fig. 9. Ten InSAR DEM height profiles compared with GLAS ground tracks (the attached numbers correspond to those in Fig. 5). This figure shows the reduction procedure from the original InSAR DEM (dark blue) to GLAS-corrected InSAR DEM (yellow) profiles. Height scale is common for all profiles from 2 through 10. The number of 500 points corresponds to 30 km. (For interpretation of the references to colour in this figure legend, the reader is referred to the web version of this article.)

The height difference between the InSAR DEM and GLAS DEM profiles was minimized by an iterative approximation using Eqs. (8)–(10), and the GLAS-corrected InSAR DEM heights (yellow dots in Fig. 9, as calculated using Eq. (9)) have an overall rms error of ±31.1 m. The yellow dots define a line of about 30 m thick, reflecting the rms error. There is no systematic trend in the misfit among profiles 2–10.

Fig. 10 shows comparison of GLAS-corrected InSAR DEM heights with the ground-survey heights conducted by JARE-28. In Fig. 10, dark blue triangles represent InSAR DEM heights along the ground-survey L-Route. Calibration using GLAS heights gives the corrected InSAR DEM heights (yellow triangles). Compared with the ground-survey heights (red triangles), the results after GLAS-correction yield a good consistency, with an rms of ±22.3 m for the L38–L121 portion, although a large negative bias of 84.0 m remains for the L2–L37 portion (labeled "correction insufficient" in Fig. 10; see also Table 4).

7. Discussion

7.1. Error modeling using a quadratic function

Tobita et al. (1998) demonstrated that estimation error in the horizontal component of the baseline length produces non-topographic pseudo-fringes of

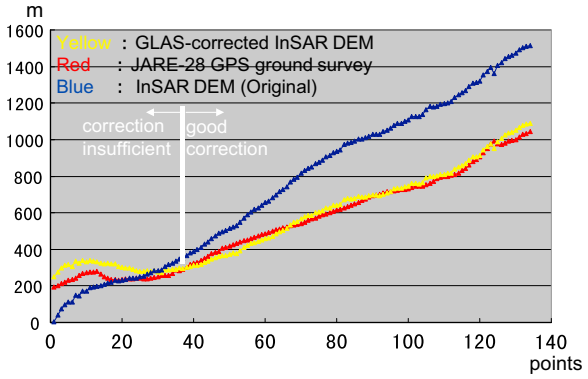

Fig. 10. Comparison of InSAR DEM heights with JARE-28 ground-survey heights. InSAR DEM heights (blue triangles) were corrected to GLAS-corrected InSAR DEM heights (yellow triangles). Compared with the ground-survey heights (red triangles), the latter have a good consistency of ±22.3 m rms for the L38–L121 portion (data labeled 'good correction'). (For interpretation of the references to colour in this figure legend, the reader is referred to the web version of this article.)

a quadratic function in the range direction and of a linear function in the azimuth direction. The authors named these pseudo-fringes a "Kamaboko function" because of its resemblance to the shape of *Kamaboko*—a processed seafood product popular in Japan. The periphery of the Antarctic ice sheet generally follows a parabolic (Kamaboko-like) shape in a north–south direction. Although non-topographic fringes in the radar (range–azimuth) coordinates are mixed up with geographically rotated trends of surface features in the polar stereographic projection coordinates (see the rotation of geographic x–y coordinates against the range–azimuth coordinates in Fig. 5), the height errors in the InSAR DEM may well be expressed by the quadratic function in Eq. (7).

The least squares estimate obtained by Eq. (8) gives the most probable set of coefficients a_0–f_0, as shown in the first row of Table 5. This procedure means that the InSAR DEM grids are adjusted such that they gradually approximate the GLAS DEM values. The iterative step in minimizing the revised Eq. (8) results in Eq. (10). The criterion considered in terms of stopping the iteration is the degree of reduction in the total rms; in our case, the rms value decreased from ±31.1 m (first step) to ±24.8 m (second step), but remained at ±24.8 m after the third (final) step. Therefore, we stopped the iteration after this third step. The corresponding values of the a_0–f_0 coefficients at each step are summarized in the second and third rows of Table 5.

The GLAS-corrected InSAR DEM height profiles deviate from the ground-control profiles by a long-wavelength separation (Figs. 9 and 10). However, a trial function of higher-order (third- and fourth-order) terms did not reduce the overall rms error or improve this separation trend, and we decided against any further simulations.

7.2. Estimate of horizontal coordinate errors in the final InSAR DEM grids

There exist three error terms for the horizontal coordinates in the obtained InSAR DEM grids. The first term for geometric correction is derived from uncertainty in the position, being ±2 pixels (±100 m). The second term is derived from the absolute position error of ±200 m propagated from the location error of the RAMP image (e.g., Jezek and RAMP Product Team, 2002). The third term is derived from the foreshortening inherent in the InSAR data. The InSAR-related height error can be considered to consist of the constant offset and the higher-order undulation. Although bias-related horizontal error can be absorbed in the first term of the geometric correction error, the higher-order undulation-related error, δ_H, is independent of the first term and can be estimated as follows:

$$\delta_H = \delta V / \tan\theta, \tag{11}$$

where δV is the higher-order height error and θ is the incidence angle of the transmitted SAR microwave. Given that the final δV is ±24.8 m and the value of θ of ERS-1 onboard SAR is 23°, δ_H is estimated to be ±58.3 m based on Eq. (11). Consequently, the overall horizontal error derived from the three terms can be roughly estimated as $\delta_H = \pm(100^2 + 200^2 + 60^2)^{1/2} = \pm 230$ m.

Table 5
Iteratively obtained values of coefficients (using Eq. (10)) and rms error obtained using Eq. (8).

	a_0	b_0	c_0	d_0	e_0	f_0	rms (m)
1st	−2.99614E−04	1.236890	−6.99615E−05	−0.38857	1.39310E−04	−514.47	±31.1 m
2nd	−1.81245E−04	0.50105	7.57123E−06	0.476997	−6.99942E−05	−716.53	±24.8 m
3rd	−1.68007E−04	0.585523	2.36054E−05	0.432257	−5.40431E−05	−1038.9	±24.8 m

7.3. Comparison with the results of other studies

7.3.1. King Edward VII Peninsula in West Antarctica

Baek et al. (2005; hereafter referred to as Baek2005) sought to validate an InSAR DEM using GLAS/ICESat for the area of the King Edward VII Peninsula (76.5–77.5°S, 153–156°W), West Antarctica. Baek2005 adopted the four-pass differential ERS-1/-2 InSAR technique (e.g., Joughin et al., 1996) because it can accurately refine the baseline vector, which is critical to the reliability of the DEM. Baek2005 used GLAS data as ground-truth measurements, with an rms height error of approximately 5 cm and a horizontal footprint with an accuracy of ±10 m (e.g., Zwally et al., 2003). Baek2005 reported an overall height consistency of ±6 m between the two data sets, although localized residual discrepancies in elevation occurred between the InSAR DEM and GLAS altimetry profiles.

The four-pass differential InSAR of ERS-1/-2 is a rare case for most of the East Antarctic ice sheet, as shown by Doi et al. (1997). For the 3.5 months of the ERS-1/-2 tandem mission, only one pair of SAR data was observed for most of the region, including our test area shown in Fig. 1.

The limited accuracy obtained in the present study (±24.8 m; Table 5) compared with ±6 m achieved by Baek2005 may reflect inaccurate determination of the baseline vector using just this single pair of InSAR data. Another factor may be the instability of GLAS measurements over the sloping ice sheet (elevation change of 1000 m), as the test area considered by Baek2005 was relatively flat (elevation change of 200 m).

7.3.2. Penetration of C-band radar waves into snow/ice

Rignot et al. (2001) examined the penetration of radar and laser signals into the ice sheet based on the results of numerous *in situ* measurements. The authors reported that laser altimetry measures the surface of snow/ice, whereas radar (SAR) penetrates into the snow/ice cover. The depth of C-band (ERS-1/-2) radar penetration is generally small (1–2 m) for exposed ice, but up to 10 m for dry, cold firn. Penetration depth depends on the wetness and compactness of the snow/ice cover, but it can reach several tens of meters. For the relatively flat area considered by Baek2005, the InSAR DEM profile was systematically 20–50 m lower than the GLAS profile; this bias was removed prior to validation of the InSAR DEM.

In the case of the relatively steep area considered in the present study, the bias-removed InSAR DEM heights were systematically lower than the GLAS DEM heights in the lower-elevation area (0–300 m), and higher in the higher elevation area (300–1000 m).

These trends were corrected in the iterative approximation procedure using the GLAS height profiles, but there remained a long-wavelength separation of the GLAS-corrected InSAR DEM heights from the GLAS heights. It is unclear whether this long-wavelength separation is related to the nature of penetration of radar waves into snow/ice, because the final topographic error (±24.8 m) is twice as large as the probable penetration depth (bias) of 10 m.

7.3.3. Comparison with superconducting gravity observations at Syowa Station

Although the absolute height accuracy of InSAR DEM grids is limited to ±24.8 m, it may be possible to

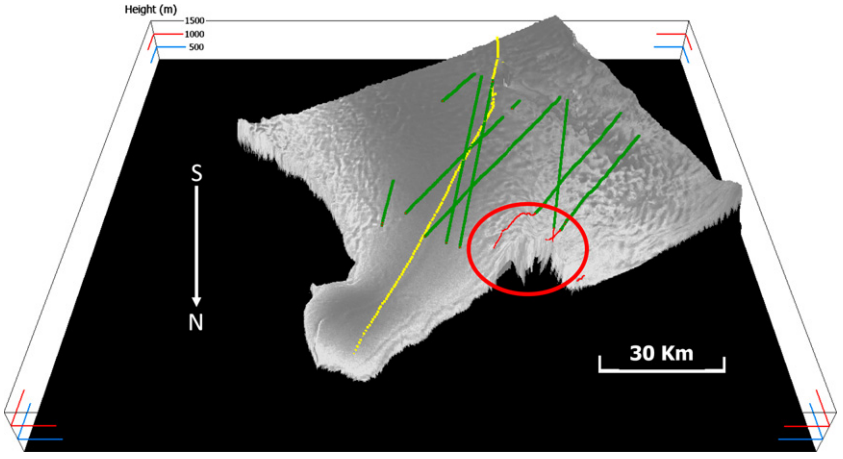

Fig. 11. Oblique aerial view (from the coast to inland areas) of the study area. Green lines are GLAS profiles, yellow dots represent the ground-survey profile measured by JARE-28, and the red circle indicates the area of high ice flow velocity with erroneous DEM heights. (For interpretation of the references to colour in this figure legend, the reader is referred to the web version of this article.)

estimate height change using yearly-obtained DEMs with an absolute accuracy that is an order of magnitude better than that of InSAR DEM grids; i.e., with a relative accuracy of ±2 m. Because the height change of the ice sheet can be converted to change in ice mass by introducing an appropriate *in situ* density−depth profile of the surface snow/ice, the change in ice mass can then be converted to the gravitational effects on the superconducting gravimeter at Syowa Station (see Fig. 1 for the location of this station) and compared with the non-tidal gravity variations. A preliminary analysis (Doi et al., in press) identified promising features for explaining this non-tidal variation, which may be associated with the GLAS-corrected InSAR DEM volume change of the nearby ice sheet.

8. Conclusion

By interpolating GLAS/ICESat 500 m DEM grids onto heights measured during a ground traverse survey along the L-Route in the area of the Breivika−Asuka Station, we were able to assess the accuracy of GLAS measurement heights. For the lower-elevation range of 0−250 m, GLAS heights differed systematically (by 40−100 m) from the traverse survey heights, which had an accuracy of 2 m. For most of the remaining elevation range (300−1000 m), the two sets of height data were consistent within ±12.4 m.

Using ERS-1/-2 SAR tandem data, we produced InSAR 50 m DEM grids for the area around Breivika−Asuka Station. The InSAR DEM heights were corrected by referring to GLAS/ICESat 500 m DEM grids as ground-control data with an allowance of ±12.4 m in overall height error. The height difference was assumed to have a quadratic function for rectangular polar stereographic coordinates with six coefficients, and the most probable estimate of the parameter set was iteratively approximated by applying a least squares method. The overall height error was ±284 m before correction; after correction, the associated errors decreased to ±24.8 m. The absolute error in the horizontal coordinates (grids) was ±230 m, but the relative horizontal error was less than the 50 m grid spacing. An oblique aerial view (from the coast to inland areas) of the study area is shown in Fig. 11.

Comparison of the GLAS-corrected InSAR DEM heights (yellow dots in Fig. 10) with the ground-truth heights (red dots in Fig. 10) along the survey route revealed a ±22.3 m overall discrepancy for the elevation range of 300−1000 m. There exists a factor 2 degradation of accuracy in the GLAS-corrected InSAR DEM grid heights against the ±12.4 m overall accuracy of GLAS height measurements confirmed by the height profile derived from the ground survey.

A large, systematic negative bias in GLAS/ICESat heights over the low-elevation area (0−300 m) may be associated with the inaccurate tracking of laser measurements across the transition zone from sea to sloping land. However, the main reason for the error in the InSAR DEM grid heights is distortion of topographic fringes arising from the use of a single, short baseline InSAR.

The error in relative elevation change indicated by yearly InSAR DEM grids may be about one-tenth of the absolute height error (i.e., ±2 m). A DEM with an accuracy of 2 m would enable the detection of temporal changes in the ice mass in coastal regions of Antarctica. This ice mass change could be compared with non-tidal gravity variations observed by a superconducting gravimeter at Syowa Station.

Acknowledgments

The ERS-1/-2 data used in this study were acquired at Syowa Station by the JARE-37 satellite receiving team. The European Space Agency retains ownership of the original data, which were processed and provided by the Japan Aerospace Exploration Agency/Earth Observation Center (JAXA/EOC) under an agreement between JAXA and NIPR. The authors express their sincere thanks for this contribution. This research was partly financed by a Grant-in-Aid for Scientific Research (C) (2) No. 14580556 (P.I.: K. Shibuya) from the Japan Society for the Promotion of Science (JSPS).

References

ADD Consortium, 2000. Antarctic Digital Database, Version 3.0. Database, Manual and Bibliography. Scientific Committee on Antarctic Research, Cambridge, 93 pp.

Atwood, D.K., Guritz, R.M., Muskett, R.R., Lingle, C.S., Sauber, J.M., Freymueller, J.T., 2007. DEM control in Arctic Alaska with ICESat laser altimetry. IEEE Trans. Geosci. Remote Sens. 45 (11), 3710−3720.

Baek, S., Kwoun, O.-I., Braun, A., Lu, Z., Shum, C.K., 2005. Digital elevation model of King Edward VII Peninsula, West Antarctica, from SAR interferometry and ICESat laser altimetry. IEEE Geosci. Remote Sens. Lett. 2 (4), 413−417.

Carabajal, C.C., Harding, D.J., 2005. ICEsat validation of SRTM C-band digital elevation models. Geophys. Res. Lett. 32, L22S01. doi:10.1029/2005GL023957.

Csatho, B., Ahn, Y., Yoon, T., van der Veen, C.J., Vogel, S., Hamilton, G., Morse, D., Smith, B., Spikes, V.B., 2005. ICESat measurements reveal complex pattern of elevation changes on Siple Coast ice streams, Antarctica. Geophys. Res. Lett. 32, L23S04. doi:10.1029/2005GL024289.

DiMarzio, J., Brenner, A., Schutz, R., Shuman, C.A., Zwally, H.J., 2007. GLAS/ICESat 500 m Laser Altimetry Digital Elevation

Model of Antarctica. National Snow and Ice Data Center, Boulder. Digital media.

Doi, K., Shibuya, K., Aoyama, Y., Ikeda, H., Fukuda, Y. Observed gravity change at Syowa Station Induced by Antarctic Ice Sheet Mass Change. IAG Symposia, Springer, in press.

Doi, K., Shibuya, K., Ozawa, T., Nakagawa, H., 1997. SAR data acquisitions at Syowa station in Antarctica. In: Forsberg, R., Feissel, M., Dietrich, R. (Eds.), IAG Symposia 119. Geodesy on the Move; Gravity, Geoid, Geodynamics, and Antarctica. Springer-Verlag, Berlin, pp. 529–534.

Fricker, H.A., Padman, L., 2006. Ice shelf grounding zone structure from ICESat laser altimetry. Geophys. Res. Lett. 33, L15502. doi:10.1029/2006GL026907.

Fujii, Y., Motoyama, H., Azuma, N., 1995. Glaciological Data Collected by the 30th, 31st and 32nd Japanese Antarctic Research Expeditions in 1989–1991, 89 pp. In: JARE Data Reports, No. 201(Glaciology 22). Natl Inst. Polar Res., Tokyo.

Fujita, M., Iga, A., Okita, T., 1987. Design of the GPS interferometer. In: Paper presented at the International Union of Geodesy and Geophysics (IUGG) XIX General Assembly, Aug. 9–22, Vancouver, B.C., Canada.

Gamma Remote Sensing, 2007. Gamma Interferometric SAR Processor –ISP. User's Guide, Bern.

Goldstein, R.M., Engelhardt, H., Kamb, B., Frolich, R.M., 1993. Satellite radar interferometry for monitoring ice sheet motion: application to an Antarctic ice stream. Science 262, 1525–1530.

Hanssen, R., 2001. Radar Interferometry: Data Interpretation and Error Analysis (Remote Sensing and Digital Image Processing). Kluwer Academic Pub., Amsterdam, 328 pp.

Jezek, K., RAMP Product Team, 2002. RAMP AMM-1 SAR Image Mosaic of Antarctica. Alaska Satellite Facility, Fairbanks, in Association With The National Snow and Ice Data Center, Boulder. Digital media.

JMR Instruments Inc., 1977. The JMR-1 Doppler Survey Set, Description and Application. Chatsworth, CA, 24 pp. (JMR Document No. 73288-3).

Joughin, I., Winebrenner, D., Fahnestock, M., Kwok, R., Krabill, W., 1996. Measurement of ice-sheet topography using satellite-radar interferometry. J. Glaciol. 42, 10–22.

Lemoine, F., Smith, D.E., Smith, R., Kunz, L., Pavlis, E.C., Pavlis, N.K., Klosko, S.M., Chin, D.S., Torrence, M.H., Williamson, P.G., Cox, C.M., Rachlin, K.E., Wang, Y.M., Kenyon, S.C., Salman, R., Trimmer, R., Rapp, R.H., Nerem, R.S., 1997. The Development of the NASA GSFC and NIMA Joint Geopotential Model. In: IAG Symp. No. 117, ''Gravity, Geoid and Marine Geodesy''. Springer-Verlag, Berlin, pp. 461–469.

Liu, H., Jezek, K., Li, B., Zhao, Z., 2001. Radarsat Antarctic Mapping Project Digital Elevation Model Version 2. National Snow and Ice Data Center, Boulder. Digital media.

Nishio, F., Ohmae, H., 1989. Glaciological Research Program in East Queen Maud Land, East Antarctica. Part 8, 1986–1987, 59 pp. In: JARE Data Reports, No. 148(Glaciology 17). Natl Inst. Polar Res., Tokyo.

Rignot, E., 1996. Tidal motion, ice velocity and melt rate of Petermann Gletscher, Greenland, measured from radar interferometry. J. Glaciol. 42, 476–485.

Rignot, E., Casassa, G., Gogineni, S., Kanagaratnam, P., Krabill, W., Pritchard, H., Rivera, A., Thomas, R., Turner, J., Vaughan, D., 2005. Recent ice loss from the Fleming and other glaciers, Wordie Bay, west Antarctic peninsula. Geophys. Res. Lett. 32, L07502. doi:10.1029/2004GL021947.

Rignot, E., Echelmeyer, K., Krabill, W., 2001. Penetration depth of interferometric synthetic-aperture radar signals in snow and ice. Geophys. Res. Lett. 28 (18), 3501–3504.

Schutz, B.E., Zwally, H.J., Shuman, C.A., Hancock, D., DiMarzio, J.P., 2005. Overview of the ICESat mission. Geophys. Res. Lett. 32, L21S01. doi:10.1029/2005GL024009.

Shibuya, K., Fukuda, Y., 1999. Gravity Survey Along the L- and AB-Routes, East Dronning Maud Land, Antarctica, pp. 16–30. In: JARE Data Rep. 237. Natl. Inst. Polar Res., Tokyo.

Shibuya, K., Doi, K., Aoki, S., 1999. Precise determination of geoid height and free-air gravity anomaly at Syowa Station, Antarctica. Earth Planets Space 51, 159–168.

Shibuya, K., Fukuda, Y., Michida, Y., 1990. Application of GPS relative positioning for height determination above sea level in the Antarctic marginal ice zone. J. Phys. Earth 38, 147–160.

Shibuya, K., Fukuda, Y., Michida, Y., 1991. Determination of geoid height at Breid Bay, east Antarctica. J. Geophys. Res. 96 (B11), 18,285–18,294.

Shuman, C.A., Zwally, H.J., Schutz, B.E., Brenner, A.C., DiMarzio, J.P., Suchdeo, V.P., Fricker, H.A., 2006. ICESat Antarctic elevation data: preliminary precision and accuracy assessment. Geophys. Res. Lett. 33, L07051. doi:10.1029/2005GL025227.

Tobita, M., Fujiwara, S., Ozawa, S., Rosen, P.A., Fielding, J.E., Werner, C.L., Murakami, M., Nakagawa, H., Nitta, K., Murakami, M., 1998. Deformation of the 1995 north Sakhalin earthquake detected by JERS-1/SAR interferometry. Earth Planets Space 50, 313–325.

Watanabe, O., Furukawa, T., Fujita, S., 1990. Glaciological Data Collected by the 29th Japanese Antarctic Research Expedition in 1988–1989, 77 pp. In: JARE Data Reports, No. 156(Glaciology 18). Natl Inst. Polar Res., Tokyo.

Wingham, D.J., Ridout, A.J., Scharroo, R., Arthern, R.J., Shum, C.K., 1998. Antarctic elevation change from 1992 to 1996. Science 282, 456–458.

Yamanokuchi, T., Doi, K., Shibuya, K., 2005. Validation of grounding line of the East Antarctic ice sheet derived by ERS-1/2 interferometric SAR data. Polar Geosci. 18, 1–14.

Zebker, H.A., Werner, C.L., Rosen, P.A., Hensley, S., 1994. Accuracy of topographic maps derived from ERS-1 interferometric radar. IEEE Trans. Geosci. Remote Sens. 32 (4), 823–836.

Zwally, H.J., Schutz, R., Bentley, C., Bufton, J., Herring, T., Minster, J., Spinhirn, J., Thomas, R., 2003. GLAS/ICESat L2 Antarctic and Greenland Ice Sheet Altimetry Data V018, 15 October to 18 November 2003 (updated current year). National Snow and Ice Data Center, Boulder. Digital Media.

NiPR
National Institute of Polar Research

INTERNATIONAL POLAR YEAR
2007-2008